High resolution dynamic strain sensor using a polarization maintaining fiber Bragg grating

Dipen Barot, *Student Member, IEEE*, Gang Wang, and Lingze Duan, *Senior Member, IEEE*

***Abstract*—Dynamic strain sensing based on fiber Bragg gratings (FBG) has found a wide range of applications in structure health monitoring and industrial process control. Conventional approaches to enhance strain resolution upon the standard configuration have shown challenges in scaling up due to much-increased system complexity. In this report, we demonstrate a new scheme based on an FBG sensor fabricated in a polarization-maintaining fiber. By using balanced detection to suppress laser intensity noise and enhance strain signal, we have demonstrated an improvement of 28 dB in signal level, 18 dB in signal-to-noise ratio, and 20× in strain resolution when compared to the results using a regular FBG sensor. Moreover, this new sensing concept does not require complicated frequency locking systems and hence allows easy scaleup.**

***Index Terms*—Dynamic strain measurement, fiber Bragg grating sensors, polarization-maintaining fibers**

I. Introduction

Fiber-optic sensors have become a major sector in the rapidly growing sensor market, holding many advantages over conventional electronic sensors, including low cost, high sensitivity, large bandwidth, immunity to electromagnetic interference, and scalability to large networks [1]. Among various types of fiber-optic sensors, fiber Bragg gratings (FBGs) have emerged as the most important modality for local and distributed sensing of strain, temperature, vibration and pressure due to their unique capability of wavelength-encoded measurement [2,3]. In particular, FBG-based dynamic strain sensors have been widely used in smart structures and structural health monitoring applications [4,5]. These sensors typically can achieve strain resolutions at sub-microstrain ($\mu\varepsilon$) level. However, as the demand for high-resolution strain sensing continues to arise, there has been a constant effort to lower the minimum detectable strain by FBG sensors [6].

A number of techniques have been developed to improve the strain resolution of FBG sensors [7-15]. The central idea behind all these methods is to enhance wavelength selectivity, either by introducing additional wavelength discriminators or by optimizing the FBG designs to create sharper resonance peaks. Among the notable prior works, methods based on interferometric wavelength discriminators have demonstrated dynamic strain resolutions of the order of $\sim 1\ n\varepsilon/\sqrt{Hz}$ [7,8]. Locking lasers to FBG has pushed this resolution further down to $45\ p\varepsilon/\sqrt{Hz}$ (at 3 kHz) [9]. With π-phase-shifted FBG, which can produce extremely sharp resonance peaks, $\sim 5\ p\varepsilon/\sqrt{Hz}$ strain resolution has been first reported [11]. Its operating frequency was initially limited to >100 kHz. However, this high-frequency limitation has been mitigated in a recent report to $\sim 10\ p\varepsilon/\sqrt{Hz}$ strain resolution at 10 Hz [12]. Meanwhile, an ultrahigh dynamic strain resolution of $140\ f\varepsilon/\sqrt{Hz}$ (at >1 kHz) has been achieved using a π-phase-shifted FBG frequency-locked to a random distributed feedback fiber laser [13]. Another method showing great potential is slow-light FBG, which relies on a unique fabrication process to create strong apodized FBG with a series of narrow resonance peaks [14]. Such resonance features have been utilized to attain a strain resolution approaching the thermodynamic noise limit of $130\ f\varepsilon/\sqrt{Hz}$ at 1.5 kHz [15]. Despite the tremendous success by these prior efforts, the improvement in performance has come at the cost of increasing scheme complexity. Not only is highly specialized FBG fabrication necessary for some of these techniques, but sophisticated laser frequency locking, such as the Pound-Drever-Hall scheme, is also required, making these methods very difficult to scale up and significantly limiting their applicability in engineering applications.

In this paper, we take a different approach toward enhancing strain resolution. Instead of trying to maximize the strain signal by creating sharper wavelength discriminators, we aim to suppress the noise using the FBG itself. In almost all fiber-optic sensing systems, the dominant noise is laser intensity/frequency noise [16]. By creating a scenario within a single FBG where laser intensity noise becomes a common-mode noise and hence can be easily cancelled out, we are able to lower the minimum detectable strain and improve the single-to-noise ratio (SNR). To this end, we use FBGs fabricated in polarization-maintaining fibers (i.e., PM-FBGs). PM-FBGs, sometimes also referred to as HiBi-FBGs, are a common type of FBG widely available on the commercial market with very low costs [17]. Their applications in fiber-optic sensing have been well-studied, but mostly in the context of multi-parameter sensing. Because of the birefringence of polarization-maintaining (PM) fiber, a PM-FBG possesses two resonance peaks in its reflection spectrum, which correspond

This work was supported in part by the National Science Foundation under Grants ECCS-1254902 and ECCS-1606836.

Dipen Barot was with the University of Alabama in Huntsville, Huntsville, AL 35899 USA (e-mail: dkb0005@uah.edu).

Gang Wang was with the Department of Mechanical and Aerospace Engineering, The University of Alabama in Huntsville, Huntsville, AL 35899.

Lingze Duan was with the Department of Physics and Astronomy, the University of Alabama in Huntsville, Huntsville, AL 35899 USA.

978-1-7281-0615-1/19/$31.00 ©2019 IEEE

to the two orthogonal polarizations. This additional degree of freedom in polarization enables polarization-assisted characterization [18], which has found a breadth of applications in multi-dimensional and multi-parameter sensing [19-21]. However, what has been largely overlooked in the study of PM-FBGs is their potential in enhancing the resolution and SNR for the measurement of longitudinal strains. This is the focus of the current paper.

The paper is organized in the following order. We discuss principle of operation in section II. Section III describes the experiment. Results and discussions are described in section IV. Finally, a conclusion is given in section V.

II. Principle of Operation

The reflection spectrum from a PM-FBG features two resonance peaks. Their wavelengths are given by

$$\lambda_s = 2\Lambda n_{eff}^s \text{ and } \lambda_f = 2\Lambda n_{eff}^f , \quad (1)$$

where Λ is the grating period, λ_s (λ_f) and n_{eff}^s (n_{eff}^f) are the Bragg wavelength and the effective refractive index for the polarization component along the slow (fast) axis, respectively [21]. When the grating period Λ changes under longitudinal strains, both λ_s and λ_f change accordingly as suggested by (1). Since n_{eff}^s and n_{eff}^f are nearly equal and their changes due to strain are very small, both Bragg wavelengths shift toward the same direction by approximately the same amount [21].

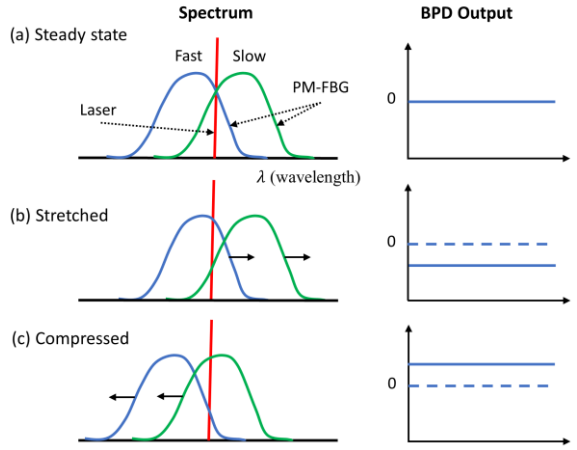

Fig. 1. Operating principle of the proposed scheme: The reflection spectrum of PM-FBG relative to laser (left) and the corresponding output of BPD (right) in (a) steady state, (b) stretched, and (c) compressed conditions.

With this basic understanding about PM-FBG, here is how the proposed scheme works: A proper PM-FBG is chosen so that its two resonance peaks share an overlapping region in the middle of them. Under the steady state (i.e., strain free), a single-wavelength interrogating laser is tuned to the crossover wavelength between the two Bragg reflection peaks, as illustrated by the left panel of Fig. 1(a). The polarization of the injected light is adjusted so that equal amount of optical power is reflected by the PM-FBG along its fast and slow axes. The two orthogonally polarized reflection signals are separately detected and the detector outputs are subtracted from each other to create a *null* under the stead state (i.e., balanced photodetection), as shown in the right panel of Fig. 1(a). When the PM-FBG is under a longitudinal strain, the two Bragg peaks shift together toward one direction, causing dislocation of the laser wavelength from the crossover point between the two peaks, as depicted by the left panels of Fig. 1(b) and (c). However, the reflected powers along the fast and the slow axes change toward opposite directions due to the opposite signs of their corresponding reflectivity slopes. This allows the balanced photodetector (BPD) to generate a large, offset-free response, as shown in the right panels of Fig. 1(b) and (c).

To further appreciate the advantages of this technique in comparison with the conventional scheme based on a regular FBG (which uses the edge of *one* Bragg peak), we note that, analytically, the power reflectivity of a PM-FBG along its fast (R_f) and slow (R_s) axes can be approximated by the following linear relations near the crossover wavelength [9]

$$R_f(\nu) = R_0 + G(\nu - \nu_0) \text{ and } R_s(\nu) = R_0 - G(\nu - \nu_0) \quad (2)$$

where ν is optical frequency, and ν_0, R_0 and G are optical frequency, power reflectivity and slope of reflectivity at the crossover wavelength, respectively. The incident optical power, which typically carries some intensity fluctuations ΔP around a nominal value P_0, can in general be written as $P = P_0 + \Delta P$. Now let us take a look at two specific scenarios. In the first one, all the incident light is polarized along the fast axis, which makes the sensor equivalent to a regular FBG. In this case, a single photodetector (SPD) is used to probe the reflected optical power and its photocurrent can be approximately expressed as

$$i_{SPD}(\nu) \approx \mathcal{R}(R_0 P_0 + R_0 \Delta P + P_0 G \Delta\nu), \quad (3)$$

where $\mathcal{R}$ is detector responsivity and $\Delta\nu \equiv \nu - \nu_0$ is frequency detuning from the crossover point due to the presence of strain. In writing (3), we have assumed both ΔP and $\Delta\nu$ are small so the second-order term is neglected. In the second case, laser frequency is positioned at the crossover point between the two Bragg peaks under steady state and the incident power is evenly split between the fast and the slow axes. Balanced detection is then used to create an output null, eliminating the constant background at the crossover wavelength. Assuming the same detector responsivity, the net photocurrent from the BPD is

$$i_{BPD}(\nu) \approx \mathcal{R} P_0 G \Delta\nu. \quad (4)$$

Once again, the second-order term has been neglected.

A comparison between (3) and (4) shows two key advantages of using a PM-FBG sensor. First, the dominant dc-offset term $\mathcal{R}R_0P_0$ is cancelled out in the BPD output. This allows the use of a large transimpedance gain when converting photocurrent into voltage, effectively raising detector resolution while helping the strain-induced signal overcome instrument noise. Secondly, the first-order contribution of laser intensity noise is also removed from i_{BPD}, making the detector much less sensitive to laser power fluctuations. As a result, the overall SNR is also expected to improve.

III. Experiment

A layout of the experimental setup is shown in Fig. 2(a). The FBG sensor is fabricated on a PANDA-type PM fiber. It has

two Bragg reflection peaks about 0.6 nm apart, with each peak having a 0.4-nm full width at half maximum (see Fig. 2(b)). A single-frequency, external-cavity diode laser operating near 1550 nm serves as the light source and its wavelength is tuned to the crossover wavelength of the two Bragg peaks, as shown in Fig. 2(b). The laser has a nominal linewidth of 50 kHz and a maximum power of 40 mW, with a wavelength tuning range from 1549.5 nm to 1550.5 nm by adjusting the temperature. The fiber-coupled laser output passes through an isolator before entering a polarization controller, which is used to set the polarization state of the interrogating light. A polarization-maintaining 50:50 coupler couples the interrogating light into the PM-FBG sensor and sends the reflected power (~100 μW) toward the output. A fiber-coupled polarization beamsplitter splits the two orthogonal polarization modes in the output, feeding them into the two photodiodes of a balanced amplified photoreceiver (Thorlabs PDB 440C). The receiver provides a transimpedance gain of 5.1×10^4 V/A. All the fibers and fiber connectors after the polarization controller are PM type so that the polarization state is preserved. In order to generate calibrated strain, the PM-FBG is epoxied on a 1.25×0.5×0.02 in. piezoelectric extension actuator, which has a charge constant of 1.26 $\mu\varepsilon$/V and a resonance frequency of 26.2 kHz.

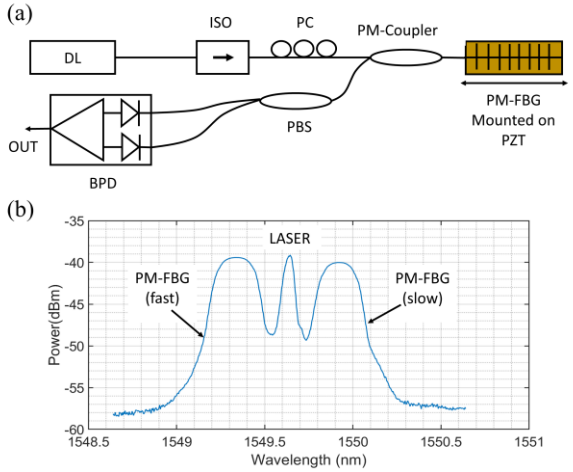

Fig. 2. (a) Schematic of the experimental setup for PM-FBG strain sensing. DL: diode laser, ISO: fiber-coupled isolator, PBS: polarization beam splitter, PC: polarization controller, PM-Coupler: polarization maintaining coupler. (b) Laser wavelength is tuned to the crossover point between the two PM-FBG Bragg peaks. The spectrum is measured by simultaneously coupling outputs from a mode-locked laser and the DL into the PM-FBG.

IV. Results and Discussions

In order to demonstrate dynamic strain measurement with the PM-FBG sensor, a sinusoidal modulation voltage is applied to the actuator and the output of the receiver is monitored using a fast Fourier transform signal analyzer (SRS SR785). Both SPD and BPD schemes are studied. In the SPD scheme, the polarization of the interrogating light is adjusted to align with one of the primary axes of the PM fiber and only one Bragg peak is involved in the sensing process. As a result, only one photodetector in the photoreceiver is used in strain measurement. In the BPD scheme, the incident polarization is adjusted to balance the BPD output when the PM-FBG is strain free. Both Bragg peaks are involved in the sensing process and both photodetectors contribute to strain measurement. Moreover, the removal of the large dc offset allows the transimpedance gain of the photoreceiver to be activated in this case.

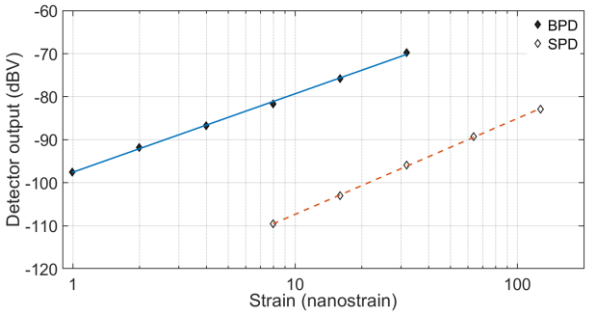

Fig. 3. Measurements of dynamic strain at 1.5 kHz with the BPD (solid) and the SPD (open) schemes. Lines represent linear fitting.

A typical set of strain measurement results is summarized in Fig. 3. Here, dynamic strain at 1.5 kHz is introduced to the PM-FBG with various amplitudes, and the sensor response is recorded with both the SPD (open diamond) and the BPD (solid diamond) configurations. Both sets of data exhibit a high degree of linearity on the log-log scale with roughly a 20 dBV/decade slope as shown in Fig. 3. This suggests that the sensor responds to strain in a highly linear fashion. More importantly, under the same strain levels, the detector output in the BPD scheme shows a 28-dB increment compared to the case using the SPD scheme. Such a dramatic enhancement of the signal level is primarily attributed to the transimpedance gain of the BPD receiver, which is enabled due to the cancellation of the large dc background.

The minimum strain resolvable by the PM-FBG sensor is assessed by measuring the system noise floor over the frequency range of 1 Hz – 100 kHz. Fig. 4 summarizes the results with both the BPD and the SPD schemes. In both configurations, the receiver output under strain-free condition is measured with and without the interrogating light, with the latter case serving as a reference of instrument noise (see Fig. 4(a) and (b)). The corresponding strain noise floors for the two schemes, after proper calibrations based on the data shown in Fig. 3, are compared in Fig. 4(c). The BPD scheme displays clear improvement in strain resolution than the SPD scheme across several decades of frequency. The only exception, however, occurs within 20 Hz – 200 Hz, where the BPD noise is markedly higher than the SPD noise at certain frequencies. This is likely caused by the transimpedance amplifier used in the BPD configuration, which tends to channel fluctuations in the power line into the photoreceiver. Such electronic noise should in principle be easy to remove or mitigate via better power-line shielding or amplifier design. The dynamic strain resolution with the BPD scheme is 700 $p\varepsilon/\sqrt{Hz}$ at 10 Hz and 30 $p\varepsilon/\sqrt{Hz}$ at 100 kHz. This represents an improvement of a factor of 3 at 10 Hz and a factor of 20 at 100 kHz over the SPD scheme, which operates similarly as a regular FBG.

Temperature is a key factor affecting sensor stability. In the case of PM-FBG, temperature variations can lead to Bragg wavelength shift and polarization state fluctuations. Both of these effects cause the BPD to drift away from the optimum balanced state even without external strain. To verify the long-term stability of the BPD scheme, we monitor the steady-state BPD output over long periods of time after initial optimization

and find that under normal lab conditions the drift can remain very small for hours. Fig. 4(c) inset shows a typical set of data where the maximum BPD output drift over 2000 s is about 50 mV, which should not affect the BPD operation given the ±1.2-V BPD saturation voltage. Moreover, since temperature-induced fluctuations are typically *slow* changes, i.e. << 1 Hz, they are not expected to interfere with dynamic strain sensing.

SNR is another important parameter for strain sensors. We have measured the photoreceiver output spectra under a fixed amount of dynamic strain with both the BPD and the SPD configurations. Fig. 5 compares the results between these two schemes for (a) 64 $n\varepsilon$ at 85 Hz and (b) 16 $n\varepsilon$ at 1.5 kHz. In both cases, it is evident that significant improvement of SNR can be attained using a PM-FBG sensor along with balanced detection. In particular at 85 Hz, an SNR enhancement over 18 dB has been achieved as shown in Fig. 5(a). This demonstrates the effectiveness of PM-FBG sensors in enhancing SNR.

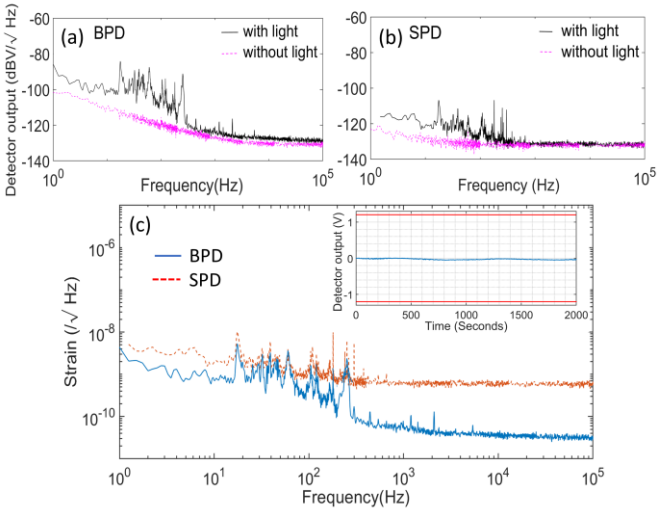

Fig. 4. Noise floors and instrument backgrounds for (a) BPD and (b) SPD schemes. (c) Noise-limited strain resolutions for BPD and SPD. Inset: long-term BPD output stability over 2000 s (red lines: BPD saturation voltages).

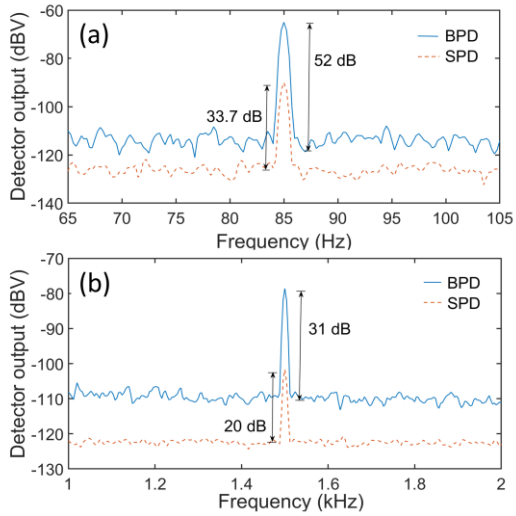

Fig. 5. Comparisons of signal-to-noise ratios between the BPD and the SPD schemes for dynamic strains of (a) 64 $n\varepsilon$ at 85 Hz and (b) 16 $n\varepsilon$ at 1.5 kHz.

V. Conclusion

Current results have demonstrated that a PM-FBG sensor is able to enhance both strain resolution and SNR compared to the case of using a regular FBG. In particular, enhancements including 28 dB in signal level, 18 dB in SNR, and 20× in strain resolution were observed by applying a BPD scheme to a PM-FBG sensor. More importantly, such improvements do not require a large overhead in system complexity (e.g., laser frequency locking), offering the method a much better scalability than conventional approaches.

References

[1] E. Udd, "Fiber optic smart structures," in *Fiber optic sensors: An introduction to engineers and scientists*, 1st ed., New York 10158-0012, NY, USA: John Wiley & Sons Ltd, 1991, ch. 14, pp. 436-467.

[2] Y. J. Rao, "In-fiber Bragg grating sensors," *Meas. Sci. Technol.*, vol 8, pp 355–375, 1997.

[3] A. Kersey, M. Davis, H. Patrick, M. LeBlanc, K. Koo, C. Askins, M. Putnam, and E. Friebele, "Fiber Grating sensors," *J. of Lightwave Technol.*, vol 15, no. 8, pp 1442-1463, Aug 1997.

[4] M. Majumder, T. K. Gangopadhyay, A. K. Chakraborty, K. Dasgupta, and D. K. Bhattacharya, "Fibre Bragg gratings in structural health monitoring - present status and applications," *Sens. Actuat. A*, vol 147, pp 150-164, April 2008.

[5] Y. J. Rao, "Recent progress in applications of in-fiber Bragg grating sensors," *Opt. Lasers Engng.*, Vol 31, pp 297-324, 1999.

[6] J. M. López-Higuera, C., L. R. Rodriguez, A. Q. Incera, A. Cobo, "Fiber optic sensors in structural health monitoring," *J. of Lightwave Technol.*, vol 29, no. 4, pp 587-608, Feb 2011,

[7] A. D. Kersey, T. A. Berkoff, and W. W. Morey, "High-Resolution Fiber-grating based strain sensor with interferometric wavelength-shift detection," *Electr. Lett.*, vol 28, no. 3, pp 236-238, Jan 1992.

[8] M. Song, S. Yin, and P. B. Ruffin, "Fiber Bragg grating strain sensor demodulation with quadrature sampling of a Mach-Zehnder interferometer," *Appl. Opt.*, vol. 39, no. 7, pp 1106-1110, Mar. 2000.

[9] B. Lissak, A. Arie, and M. Tur, "Highly sensitive dynamic strain measurements by locking lasers to fiber Bragg gratings," *Opt. Lett.*, vol. 23, no. 24, pp. 1930-1932, Dec 1998.

[10] G. Gagliardi, M. Salza, P. Ferraro, and P. De Natale, "Fiber Bragg-grating strain sensor interrogation using laser radio-frequency modulation," *Opt. Express*, vol. 13, no. 7, pp. 2377-2384, Mar. 2005.

[11] D. Gatti, G. Galzerano, D. Janner, S. Longhi, and P. Laporta, "Fiber strain sensor based on a π-phase-shifted Bragg grating and the Pound-Drever-Hall technique," *Opt. Express*, vol. 16, no. 3, pp 1545-1550, Jan 2008.

[12] J. Chen, Q. Liu, X. Fan, and Z. He, "Ultrahigh resolution optical fiber strain sensor using dual Pound–Drever–Hall feedback loops," *Opt. Lett.*, vol. 41, no. 5, pp 1066-1069, March 2016.

[13] P. Liu, W. Huang, W. Zhang, and F. Li, "Ultrahigh resolution optic fiber strain sensor with a frequency-locked random distributed feedback fiber laser," *Opt. Lett.*, vol. 43, no. 11, pp 2499-2503, May 2018.

[14] G. Skolianos, A. Arora, M. Bernier and M. Digonnet, "Slow light in fiber Bragg gratings and its applications," *J. Phys. D: Appl. Phys.*, vol. 49, 2016.

[15] G. Skolianos, A. Arushi, M. Bernier, and M. J. F. Digonnet, "Photonics sensing at the thermodynamic limit," *Opt. Lett.*, vol 42, no. 10, pp 2018-2021, May 2017.

[16] L. Duan, "Thermal noise-limited fiber-optic sensing at infrasonic frequencies," *IEEE J. Quantum Electron.*, vol. 51, no. 2, Feb 2015.

[17] J. Noda, K. Okamoto, and Y. Sasaki, "Polarization-maintaining fibers and their applications," *J. of Lightwave Tech.*, vol. 4, no. 8, pp 1071-1089, Aug 1986.

[18] C. Caucheteur, T. Guo, and J. Albert, "Polarization-Assisted fiber Bragg grating sensors: Tutorial and Review," *J. of Lightwave Tech.*, vol 35, no. 16, pp 3311-3322, Aug 2017.

[19] C. M. Lawrence, D. V. Nelson, and E. Udd, "Measurement of transverse strains with fiber Bragg gratings," in *Proc. SPIE 3042, Smart Structures and Materials 1997: Smart Sensing, Processing, and Instrumentation*, San Diego, CA, USA, 1997, pp. 218-228. doi: 10.1117/12.275739

[20] E. Udd, "Review of multi-parameter fiber grating sensors," *Proc. SPIE 6770, Fiber Optic Sensors and Applications V*, 2007, pp. 1-10.

[21] G. Chen, L. Liu, H. Jia, J. Yu, L. Xu, and W. Wang, "Simultaneous strain and temperature Measurements with fiber Bragg grating written in novel Hi-Bi optical fiber," *IEEE Photon Technol. Lett.*, vol. 16, no. 1, pp 221-223, Jan 2004.